

Doping in Carbon Nanotubes Probed by Raman and Transport Measurements

Anindya Das,¹ A. K. Sood,¹ A. Govindaraj,² A. Marco Saitta,³ Michele Lazzeri,³ Francesco Mauri,³ and C. N. R Rao²

¹Department of Physics, Indian Institute of Science, Bangalore 560012, India

²Chemistry Physics of Materials Unit, Jawaharlal Nehru Centre for Advanced Scientific Research, Bangalore 560064, India

³IMPIC, Universités Paris 6 et 7, CNRS, IPGP, 140 rue de Lourmel, 75015 Paris, France

(Received 4 April 2007; published 25 September 2007)

In situ Raman experiments together with transport measurements have been carried out on carbon nanotubes as a function of gate voltage. In metallic tubes, a large increase in the Raman frequency of the G^- band, accompanied by a substantial decrease of its linewidth, is observed with electron or hole doping. In addition, we see an increase in the Raman frequency of the G^+ band in semiconducting tubes. These results are quantitatively explained using *ab initio* calculations that take into account effects beyond the adiabatic approximation. Our results imply that Raman spectroscopy can be used as an accurate measure of the doping of both metallic and semiconducting nanotubes.

DOI: 10.1103/PhysRevLett.99.136803

PACS numbers: 73.63.Fg, 63.20.Kr, 71.15.Mb, 78.67.Ch

Single wall carbon nanotubes (SWNTs) are one-dimensional nanostructures with fascinating electronic, elastic, and chemical properties [1,2], with distinct possibility of applications in nanoelectronics [3], biological, chemical, and flow sensors [4], etc. In many of these applications, the determination of the doping level in SWNTs is a crucial issue. Raman spectroscopy is one of the most important characterization techniques. Low-energy features (~ 100 – 200 cm^{-1}), due to the radial breathing mode (RBM), are used to determine diameter and chirality of a SWNT [1]. Higher-energy modes, near the graphite Raman G band (~ 1580 cm^{-1}), are often used to distinguish between semiconducting and metallic tubes.

In particular, G bands in semiconducting tubes are termed as G^+ (~ 1590 cm^{-1}) and G^- (~ 1567 cm^{-1}) for LO (axial) and TO (circumferential) modes [1,5,6], respectively. For metallic tubes, G^+ (~ 1580 cm^{-1}) and G^- (~ 1540 cm^{-1}) peaks are due to TO (circumferential) and LO (axial) modes [5–7], the opposite of the semiconducting case. Because of the electron-phonon coupling (EPC) interaction [7], the G^- linewidth in metallic tubes is usually broader (~ 60 cm^{-1}) than that in semiconducting tubes (~ 10 cm^{-1}).

The phonons associated with the Raman G band in graphene and with the G^- in metallic SWNTs are affected by an important Kohn anomaly (KA) [5–8]. In graphene, because of the KA, the G band undergoes a measurable upshift by changing the Fermi level with a field-effect device [9,10]. That is, in graphene, the G -band frequency can be used to measure the actual doping. Since the origin of the KAs in graphene and metallic SWNTs are very similar, one could expect similar effects in metallic SWNTs [11]. Some results on the electrochemical doping of nanotubes are already available. In semiconducting tubes, it has been seen that the G^+ modes shift by a small amount ~ 1.5 cm^{-1}/V [12,13] to higher (lower) frequencies on hole (electron) doping. In metallic tubes, the Raman G^- modes harden for both electron and hole doping by 7 cm^{-1}

for a V_g of -1 and $+1$ V [14–16]. Reference [17] qualitatively attributed the frequency shift of metallic tubes to the KA. However, the shift of the Fermi level, a key parameter to understand the results, so far has not been quantified.

In this work, we demonstrate that the shift of the G bands can be used to measure the doping level not only in metallic but also in semiconducting nanotubes. This is done by performing a combined Raman and electron-transport experiments and by comparison with *ab initio* calculations based on density functional theory (DFT). We use electrochemical gating of the nanotubes with a solid-polymer electrolyte to shift the Fermi level, which is quantified by electron-transport measurements. This allows a shift of the Fermi level at much smaller gate voltages as compared to SiO_2 gating [18–20].

SWNTs are synthesized by arc discharge followed by purification [21]. ac dielectrophoresis [22] is used to align and connect the nanotubes between two gold electrodes at 15 μm separation. The average diameter of the bundles connected to the electrodes is 10 – 50 nm from the scanning electron microscopy (SEM) image [Fig. 1(b)]. We have used as the gating material a solid-polymer electrolyte [19,20] prepared by dissolving LiClO_4 and PEO (1:0.12) in methanol to form a precursor. The gate is applied by placing a platinum electrode into the polymer layer. The advantage of the solid electrolyte over the electrolytes in solution phase is that it does not degrade the sample and electrodes and the gate current is extremely small ($\sim \text{nA}$) even at high gate voltages (~ 1 V). A DILOR triple grating spectrometer equipped with a charge-couple device is used to record the Raman spectra using a He-Ne (1.96 eV) laser. Figure 1(c) shows the RBM of our tubes. It has two bands with average diameter $d = 1.4$ and 1.6 nm. The laser at 1.96 eV is in resonance with E_{11}^M of tube diameter 1.4 nm and lies in between the E_{11}^M and E_{33}^S of 1.6 nm diameter tubes [23]. Therefore, Raman spectra has contributions from metallic tubes of $d = 1.4$ nm as well as from both semiconducting and metallic tubes of $d = 1.6$ nm.

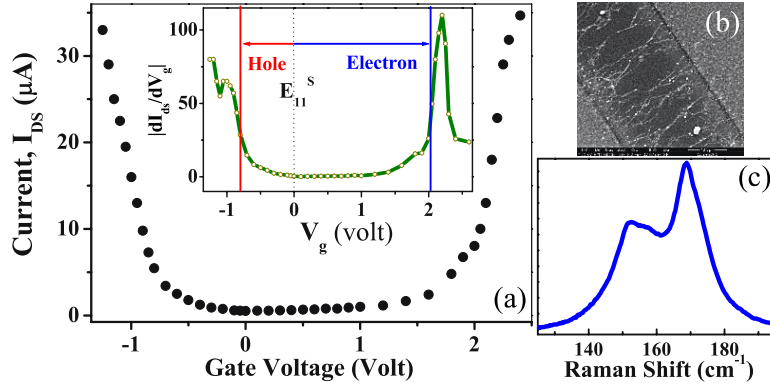


Figure 1(a) shows the ambipolar behavior of our nanotube field-effect transistor (FET) device at a drain-source voltage V_{DS} of 50 mV. At gate voltage $V_g = 0$, $I_{DS} \sim 500$ nA. The behavior of the current through the SWNT is reversible with V_g , and the leakage current is very small (~ 10 nA at $V_g \sim 2$ V). Since the current increases on either side of the starting zero V_g , we infer that the initial Fermi energy ($\epsilon_F = 0$) is at the middle of the gap of semiconducting tubes [charge neutrality point (CNP)] [20]. The sharp increase in current, as shown in Fig. 1(a), for large positive (negative) V_g is due to addition of electrons (holes) to the first van Hove singularity (VHS) on the conduction (valence) band side of the semiconducting tubes present in the sample along with the metallic tubes. The onset of this increase in current is observed for $V_g = 2.02$ and -0.8 V [inset in Fig. 1(a)]. For the semiconducting tubes of average diameter ~ 1.5 nm, $E_{11}^S \sim 0.5$ eV, and, for metallic tubes, $E_{11}^M \sim 1.8$ eV [23]. As the metallic tubes have larger energy separation between the van Hove singularities, the sharp increase in conductivity in Fig. 1(a) is governed mostly by the semiconducting tubes. Therefore, the semiconducting tubes of the sample act as an internal readout to estimate the V_g -induced ϵ_F shift. We define the proportionality factor α_e (α_h), to estimate ϵ_F at different positive (negative) gate voltages

($\epsilon_F = \alpha V_g$). For electron doping, a positive voltage of ~ 2.02 V shifts ϵ_F into the first conduction band, which is 0.25 eV from the CNP. Therefore, $\alpha_e = 0.25/2.02 = 0.12e$, and similarly $\alpha_h = 0.25/0.8 = 0.31e$. The difference between α_e and α_h is probably due to double layer formation of different ions Li^+ and ClO_4^- in PEO matrix at the interfaces.

Figure 2(a) shows the Raman spectra recorded at different V_g . A constant gate voltage is applied for 15 minutes to stabilize I_{DS} , and then the Raman spectra were recorded for next 15 minutes at the same V_g . For a V_g in the -1.25 – $+2.5$ V range, the Raman spectra as well as the source-drain current fully recover to the starting condition ($V_g = 0$) within about 1 hour after removing the gate voltage. There are three prominent Raman modes, and the spectra are fitted with three Lorentzians: $L1$ (~ 1540 cm^{-1}), $L2$ (~ 1567 cm^{-1}), and $L3$ (~ 1590 cm^{-1}). The Raman frequency, linewidth and total area thus obtained for the $L1$, $L2$, and $L3$ modes are plotted in Figs. 2(b)–2(d), as a function of V_g . Following Fig. 19 of Ref. [6], the $L1$ line is attributed to the LO mode of the metallic tubes with diameter 1.4 nm [6]. The $L1$ line can be equally well fitted by a Lorentzian or a Fano-resonance line shape. We use a Lorentzian line shape to minimize the number of fitting parameters. In our spectra, the $L2$ has a large linewidth of

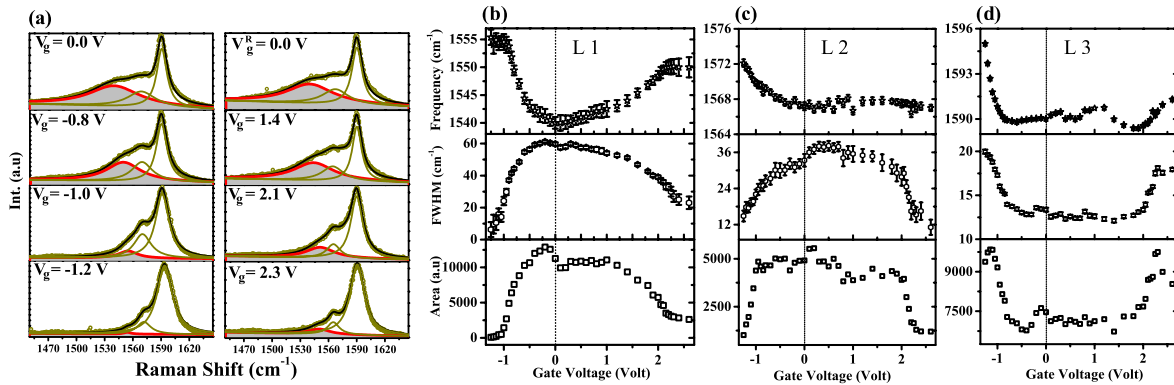


FIG. 2 (color online). (a) Tangential Raman modes of SWNTs recorded using an excitation energy of 1.96 eV at several V_g . The open circles (dark yellow) show the raw Raman spectra, and the black lines are the fitted one. The shaded Raman spectra show the LO phonon component of the metallic nanotubes. V_g dependence of (b) $L1$, (c) $L2$, and (d) $L3$ modes: Frequency (top panel), FWHM (middle panel), and total integrated area (bottom panel).

$\sim 40 \text{ cm}^{-1}$, and the doping dependence is similar to that of the $L1$ mode. Therefore, the $L2$ line is attributed to a combination of the LO mode of metallic tubes and of the TO mode of semiconducting tubes with diameter 1.6 nm (Fig. 19 of Ref. [6]). The $L3$ line is attributed to a combination of the TO of metallic and the LO of semiconducting tubes. The EPC determines an important broadening of the LO mode of metallic tubes [7]. This explains the large width of the $L1$ ($\sim 60 \text{ cm}^{-1}$) and $L2$ ($\sim 40 \text{ cm}^{-1}$) lines. The sharpness of the $L3$ line ($\sim 10 \text{ cm}^{-1}$) is explained by considering that the semiconducting LO and the metallic TO modes are not broadened by EPC and that their frequencies are almost independent from diameter (Fig. 19 of Ref. [6]).

As shown in Fig. 2(b), the largest effect is the frequency increase of the $L1$ line by 15 (10) cm^{-1} on electron (hole) doping. The substantial decrease of its linewidth is also remarkable. Both effects are due to the dependence of the KA on V_g in metallic tubes. The $L2$ line displays a similar behavior due to the metallic tubes associated with this line. The intensity of the $L1$ line (entirely due to metallic tubes) drops to zero at high doping (positive or negative). This suggests that, at high doping, the Raman signal from metallic tubes is negligible. Thus, the behavior of the $L3$ line at high doping is mostly due to semiconducting tubes. Interestingly, the frequency upshift of the $L3$ line is perfectly correlated to the I_{DS} current (Fig. 1), indicating that the $L3$ shift is due to the change of the electron (hole) populations in the conduction (valence) bands of semiconducting tubes.

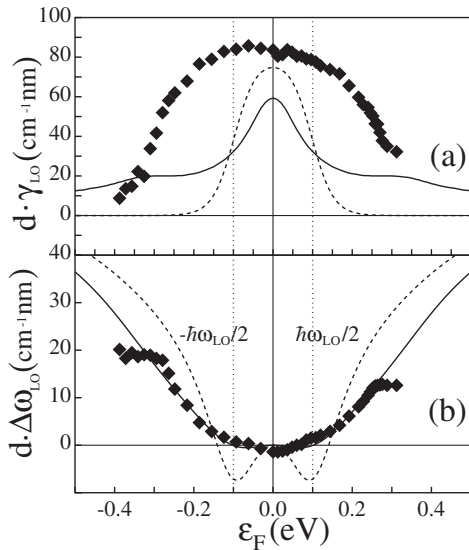


FIG. 3. G^- peak in metallic tubes: (a) Linewidth (γ_{LO} , FWHM) and (b) frequency shift ($\Delta\omega_{LO}$) as a function of the doping. The Fermi energy (ϵ_F) is zero at the charge neutrality point. γ_{LO} and $\Delta\omega_{LO}$ are multiplied by the tube diameter (d) to obtain a universal behavior. Diamonds are measurements ($L1$ line). Lines are calculations done by considering (full line) or not considering (dashed line) an inhomogeneous fluctuation of ϵ_F . ω_{LO} is the frequency of the LO phonon.

We now compare measurements with DFT calculations, done by using (i) the adiabatic Born-Oppenheimer approximation [BOA, Eq. (6) of Ref. [9]] and (ii) the time-dependent perturbation theory [TDPT, Eq. (7) of Ref. [9]] to include dynamical effects beyond the BOA. Within the BOA, the phonon frequency is obtained from the forces resulting from a *static* displacement of the atoms. However, a phonon is not a static perturbation to the system but a *dynamic* one, oscillating in time, that should be treated within the TDPT. Dynamic effects beyond the BOA are usually assumed to be negligible, but they are crucial to reproduce the Raman spectra of nanotubes and doped graphene [6,9–11]. Our DFT calculations are based on a linear response approach [24] as described in Ref. [11]. Calculations are done on a metallic (10, 10) and on a semiconducting (20, 0) tube, having diameters 1.4 and 1.6 nm, respectively. We compute the variation of the LO and the TO phonon frequency ($\Delta\omega_{LO}$ and $\Delta\omega_{TO}$) as a function of the doping. We also compute the intrinsic linewidth (γ_{LO} and γ_{TO}) due to EPC [Eq. (29) of Ref. [11]], owing to the decay of the phonon into electron-hole pairs, which is nonzero only for metallic tubes. The electronic occupations are determined according to a Fermi Dirac distribution at 315 K.

For metallic tubes, $\Delta\omega_{TO}$ and γ_{TO} are negligible, since the EPC between occupied and empty electronic states is zero [see Eq. (9) of Ref. [11]]. For diameter d larger than 1 nm, $d \times \Delta\omega_{LO}$ and $d \times \gamma_{LO}$ are universal, i.e., independent of both d and chirality [7,11]. Figure 3 reports these universal behaviors, as functions of ϵ_F , computed within the TDPT. The BOA results are not reported, since they are very similar for $\hbar\omega_{LO}/2 < |\epsilon_F| < 1.0$ eV [11]. The hard-

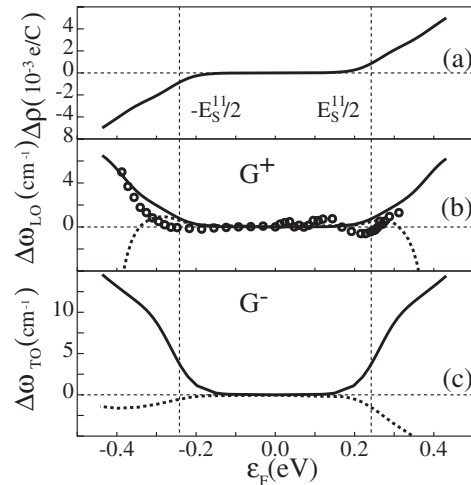


FIG. 4. G^+ and G^- peaks in 1.6 nm semiconducting tubes: (a) Theoretical charge doping per C atom. (b),(c) Frequency shift ($\Delta\omega_{LO}$, $\Delta\omega_{TO}$) as a function of the Fermi energy (ϵ_F). Open dots are measurements ($L3$ line). Dotted lines are adiabatic calculations (BOA). Full lines are our most accurate theoretical results that take into account dynamical effects (TDPT). Vertical lines are the theoretical position of the first van Hove singularities.

ening of $\Delta\omega_{LO}$ for $|\epsilon_F| > \hbar\omega_{LO}/2$ is understood by considering the modification of the electronic band structure in the presence of the LO phonon. An atomic distortion following the LO phonon pattern opens a gap at the CNP [5]. The filling of the electronic states with doping increases the energy required to open this gap, thus inducing a hardening of the LO frequency [25].

We assume that ϵ_F has a Gaussian distribution (with a standard deviation σ) to take into account the spatial fluctuation of ϵ_F in the actual device. In Fig. 3, we report the average frequency and the FWHM of the LO peak profile obtained by an ensemble of tubes with such a distribution. To include the experimental data in Fig. 3, we multiply the measured V_g by α_e and α_h . The calculations best describe the experiment with $\sigma = 0.055$ eV. The agreement between theory and measurements is excellent for $\Delta\omega_{LO}$. The theoretical LO linewidth is smaller than the experimental one, probably because of other effects, such as the finite diameter distribution.

In semiconducting tubes, $\Delta\omega_{LO}$ and $\Delta\omega_{TO}$ depend on the positions of the band edges, i.e., on d and, to a lesser extent, on the chirality. Figure 4 shows $\Delta\omega_{LO}$ and $\Delta\omega_{TO}$ computed within the BOA and the TDPT. Within the more accurate TDPT, $\Delta\omega_{LO}$ and $\Delta\omega_{TO}$ upshift when ϵ_F reaches the VHS. To understand this behavior, we have to consider how the electrons screen a phonon vibration. The electronic screening can be expressed in terms of *interband* and *intraband* EPC transitions between electronic states [9]. Within the TDPT, only the *interband* transitions between occupied valence and empty conduction electronic states contribute [Eq. (7) of Ref. [9]]. By doping the tube, the valence (conduction) band is emptied (filled). Both processes correspond to a reduction of the number of allowed transitions. The consequent reduction of the screening upshifts ω . The shift is more pronounced for the TO phonon that has a larger EPC for transition between the valence and conduction band edges. Within the BOA, the presence of *intraband* transitions [second line of Eq. (6) of Ref. [9]] contrasts the hardening due to *interband* transition [9,11].

The G^- of both metallic and semiconducting tubes are affected in a different way by V_g . Thus, the behavior of G^- of semiconducting tubes in the $L2$ line cannot be separated from that of metallic tubes. We can instead directly compare the theoretical $\Delta\omega_{LO}$ with the $L3$ line, since, at small doping, the position of the G^+ of both metallic and semiconducting tubes does not depend on V_g , and, at large doping, the metallic-tube intensity vanishes. TDPT calculations for the LO mode compare very well with the measured behavior of the $L3$ line that we report in Fig. 4 using the transport-derived ratios α_e , α_h . At the minimum V_g , $L3$ upshifts by ~ 5 cm^{-1} . According to the TDPT, this corresponds to a doping of 4.0×10^{-3} holes per C atom and to a -0.15 eV shift of ϵ_F below the first VHS.

In summary, by combining transport, *in situ* Raman experiments, and *ab initio* calculations, we quantified the effect of the doping on the phonons in carbon nanotubes.

By electron and hole doping, the Raman G^- peak of metallic tubes and both the G^- and the G^+ of semiconducting tubes harden. Moreover, the G^- linewidth of metallic tubes narrows. Important consequences of the present results are as follows: (i) The metallicity of the system is not always associated with the presence of a broad G^- peak, as often assumed. Indeed, in a doped metallic tube, the G^- -peak width can be much smaller than in the undoped case if the Fermi level is far from the π band crossing. (ii) Given the strong dependence of the Raman G bands on the Fermi energy, Raman spectroscopy can be used as an accurate measure of the doping of both metallic and semiconducting nanotubes, with important technological implications for nanoelectronics.

A. K. S. thanks DST, India for support. Calculations were performed at IDRIS (France), Project No. CP9-61387/71387, using the QUANTUM-ESPRESSO package [26].

-
- [1] S. Reich, C. Thomsen, and J. Maultzsch, *Carbon Nanotubes: Basic Concepts and Physical Properties* (Wiley-VCH, New York, 2004).
 - [2] R. Saito, G. Dresselhaus, and M. S. Dresselhaus, *Physical Properties of Carbon Nanotubes* (Imperial College Press, London, 1998).
 - [3] S. Tans, A. Verschueren, and C. Dekker, *Nature (London)* **393**, 49 (1998).
 - [4] S. Ghosh, A. K. Sood, and N. Kumar, *Science* **299**, 1042 (2003).
 - [5] O. Dubay, G. Kresse, and H. Kuzmany, *Phys. Rev. Lett.* **88**, 235506 (2002).
 - [6] S. Piscanec *et al.*, *Phys. Rev. B* **75**, 035427 (2007).
 - [7] M. Lazzeri *et al.*, *Phys. Rev. B* **73**, 155426 (2006).
 - [8] S. Piscanec *et al.*, *Phys. Rev. Lett.* **93**, 185503 (2004).
 - [9] M. Lazzeri and F. Mauri, *Phys. Rev. Lett.* **97**, 266407 (2006).
 - [10] S. Pisana *et al.*, *Nat. Mater.* **6**, 198 (2007); J. Yan *et al.*, *Phys. Rev. Lett.* **98**, 166802 (2007).
 - [11] N. Caudal *et al.*, *Phys. Rev. B* **75**, 115423 (2007).
 - [12] M. Stoll *et al.*, *Chem. Phys. Lett.* **375**, 625 (2003).
 - [13] L. Kavan *et al.*, *J. Phys. Chem. B* **105**, 10764 (2001).
 - [14] N. Bendiab *et al.*, *Phys. Rev. B* **64**, 245424 (2001).
 - [15] C. P. An *et al.*, *Synth. Met.* **116**, 411 (2001).
 - [16] P. Corio *et al.*, *Chem. Phys. Lett.* **370**, 675 (2003).
 - [17] P. M. Rafailov *et al.*, *Phys. Rev. B* **72**, 045411 (2005).
 - [18] M. Krüger *et al.*, *Appl. Phys. Lett.* **78**, 1291 (2001).
 - [19] C. Lu *et al.*, *Nano Lett.* **4**, 623 (2004).
 - [20] G. P. Siddons *et al.*, *Nano Lett.* **4**, 927 (2004).
 - [21] S. R. C. Vivekchand *et al.*, *Small* **1**, 920 (2005).
 - [22] R. Krupke *et al.*, *Science* **301**, 344 (2003).
 - [23] T. Michel *et al.*, *Phys. Rev. B* **75**, 155432 (2007).
 - [24] S. Baroni *et al.*, *Rev. Mod. Phys.* **73**, 515 (2001).
 - [25] The behavior of $\Delta\omega_{LO}$ in metallic tubes can be equally understood within perturbation theory, in terms of interband electronic transitions, as we explained in Ref. [11]. Here we adopt this approach to interpret the behavior of the semiconducting tubes.
 - [26] <http://www.pwscf.org>.